



Removal of tetracycline and rhodamine from aqueous systems by pristine biochar derived from poultry manure

Martina Mercurio^a, Sunday Joseph Olusegun^b, Krystyna Malińska^{c,*},
Katarzyna Wystalska^c, Jolanta Sobik-Szołtysek^c, Agnieszka Dąbrowska^b,
Paweł Krysiński^b, Magdalena Osiał^{d,*}

^aDepartment of Chemistry, Sapienza University of Rome, Ple A. Moro 5, 00185 Rome, Italy, email: martina.mercurio@uniroma1.it

^bFaculty of Chemistry, University of Warsaw, Pasteura 1, 02-093 Warsaw, emails: sjolusegun@gmail.com (S.J. Olusegun),
agnieszka.dabrowska@uw.edu.pl (A. Dąbrowska), pakrys@chem.uw.edu.pl (P. Krysiński)

^cFaculty of Infrastructure and Environment, Częstochowa University of Technology, Dąbrowskiego 73, 42-201 Częstochowa, Poland,
emails: krystyna.malinska@pcz.pl (K. Malińska), katarzyna.wystalska@pcz.pl (K. Wystalska), jolanta.sobik-szoltysek@pcz.pl (J. Sobik-Szołtysek)

^dDepartment of Theory of Continuous Media and Nanostructures, Institute of Fundamental Technological Research,
Polish Academy of Sciences, Pawińskiego 5B, 02-106 Warsaw, Poland, email: mosial@ippt.pan.pl

Received 5 October 2022; Accepted 17 December 2022

ABSTRACT

In this work, we investigated the potential of pristine biochar (obtained from poultry manure by pyrolysis at 725°C in a laboratory pyrolysis reactor under N₂ environment) as an efficient adsorbent for removing tetracycline (TC) and rhodamine 6G (R6G) from aqueous solutions. Microscopic and spectroscopic analyses demonstrated a developed surface of the investigated biochar free from toxic organic compounds that could form within the annealing. The removal of TC and R6G was analyzed with UV-vis spectrometry in the function of the pH, ionic strength, and adsorbent dosage. The maximal adsorption capacity for TC and R6G is 65 and 63 mg g⁻¹, respectively, indicating that pristine biochar from poultry manure has an excellent adsorption ability for both compounds demonstrating its high potential for removing various compounds of this type from water media. The enhanced adsorption on the investigated biochar is mainly controlled by the strong π - π and n - π interactions between the surface of the biochar and the two contaminants. The investigated poultry manure derived biochar can be a promising “green”, sustainable and carbon-rich material for low-cost and facile environmental applications, including the removal of contaminants from municipal wastewater.

Keywords: Pristine biochar; Poultry manure; Wastewater treatment; Tetracycline; Rhodamine 6G

1. Introduction

Emerging contaminants (ECs) are classified as toxic, persistent and hazardous substances found in soil and water. The presence of ECs in the environment is continuously increasing due to the rapid development of industries and technologies [1,2]. Nowadays, ECs can be found in many of our everyday products, for example, in personal

care products, inhuman and veterinary medicines, in agriculture, that is, in pesticides and fertilizers used on plants, and are so common that they are quickly released into the environment causing a potential threat to living organisms [3]. For example, according to the study carried out by [4,5], several types of pharmaceutical pollutants were found in treated drinking water. Although most drugs are significantly removed by water treatment, some amounts can

* Corresponding authors.

Presented at the 15th Scientific Conference on Micropollutants in the Human Environment, 14–16 September 2022, Częstochowa, Poland

1944–3994/1944–3986 © 2023 The Author(s). Published by Desalination Publications.

This is an Open Access article. Non-commercial re-use, distribution, and reproduction in any medium, provided the original work is properly attributed, cited, and is not altered, transformed, or built upon in any way, is permitted. The moral rights of the named author(s) have been asserted.

still be found in water, thus causing possible health risks to pregnant women and children.

The contaminants that are often detected in water include antibiotics and dyes. Antibiotics are commonly used to defeat bacterial infections in humans and animals. However, due to their wide application, antibiotics and their metabolites can be easily found in the environment, leading to a severe water pollution, and thus posing a threat to living organisms [6]. The presence of these substances in water has a catastrophic and adverse effect, for example, the development of antimicrobial resistance strains (ARS). As a result, the antibiotics become ineffective when antibiotic-resistant bacteria attack the body [7]. Antibiotic resistance of bacteria leads to the spread of diseases, and as a result, we are exposed to more severe illnesses and even death. It is estimated that about 70% of global consumption of antibiotics is used to produce food of animal origin, whereas 30% is used to treat humans. According to the prediction, the global consumption of antibiotics for veterinary medicines is to increase to 105,600 tons/y by 2030 [8].

1.1. Tetracycline

One of these antibiotics is tetracycline which is commonly used in medicine to treat humans and agriculture, for example, to suppress pathogen growth [7]. Tetracycline antibiotics (TCs) is a group of compounds including tetracycline, oxytetracycline and chlortetracycline. They consist of a tetracyclic ring system with several functional groups attached to it such as hydroxyl, methyl, keto, and dimethylamino groups. Their presence in the environment causes the formation of the ARS and can lead to its degradation and formation of harmful compounds. Despite many advantages, uncontrolled use and subsequent release in the form of excrement from both humans and animals pose a danger to the ecological environment [9]. It has been reported that tetracycline antibiotics are not easy to digest and absorb, and as a result about 50%–80% is excreted in urine or feces [9]. The literature reports that the main degradation products come from the reactions under the UV-light, pH, and other chemical compounds in aquatic systems [9–11]. However, irrespective of the degradation pathway, the degradation products can be more toxic than tetracycline and its metabolites. In this work, the removal ability of TC from aqueous solutions by biochar is studied since TC is among the three most widely used antibiotics due to its advantages such as low production cost and the possibility of being synthesized with high purity [14].

1.2. Rhodamine 6G

Aside from antibiotics, dyes are a broad group of chemical compounds that can be rapidly transferred to the environment, especially aquatic systems. Rhodamine is used in many industrial applications, for example, it is commonly used as a water tracer enabling the monitoring of the water flow [12], a fluorescent indicator in many industrial fields like food [13], pharmaceutical and even the textile [14] or cosmetic industry [15]. One of the most extensively used in dyeing of silk, nylon, wool and acrylic is Rhodamine 6G (R6G) [18]. Rhodamine 6G can be harmful, causing

significant health threats. It can irritate skin and eyes [16], induce neoplasms, acting as a carcinogenic substance [17]. In addition, other types of toxicity, such as reproductive system disorders and neurotoxicity, have been found after exposure to these dyes and thus can be present in wastewater.

The need to find efficient techniques to remove pollutants from water stems from the inability of textile industries to properly dispose of wastewater, resulting in global environmental pollution. Examples of persistent and harmful pollutants in water include organic dyes that can impart unique colors to a particular substrate due to the presence of chromophore groups within these molecules. In general, dyes are classified according to their origin (natural or synthetic), structure, and application, but those most widely used by textile industries are synthetic dyes, subdivided into azoic, direct, reactive, basic, and acid. However, inefficient dyeing processes do not ensure adequate adhesion of the dye to the fabric fibers, resulting in the release of wastewater from aquatic environments such as rivers, lakes, and streams, leading to aesthetic damage and negative impacts on the health of water bodies and soil [18].

1.3. Potential of biochar for removal of chemical dyes and pharmaceuticals

Since many chemical dyes and pharmaceuticals are detected in water it needs the effective treatment. There are many techniques applied to remove the aquatic pollutants from aqueous media, such as the application of a filtering system [18], phytoremediation of wastewater [19], photodegradation [20,21]. Recently, one of the most advanced techniques is based on the application of adsorbents demonstrating large surface-to-volume ratios like nanoparticles [22–24], nanocomposites [25,26], porous nano-structural minerals [27], and pristine and engineered biochars [8,28,29].

Biochars have been continuously attracting the attention of scientists worldwide due to their sustainability and a high potential for the removal of aquatic pollutants [30]. Biochars are carbon-rich and stable forms of charcoal [31]. They can be produced mainly through thermal conversion (i.e., pyrolysis) of all types of biomass with a limited amount or absence of oxygen [32] or microwave-assisted pyrolysis [33]. Furthermore, biochars can be obtained from not only various types of plant biomass, including woody materials, agricultural residues such as straw, corn cob and stove, rice husk, etc. [34–38], but can also be obtained from animal manure such as cow manure, poultry manure, etc. [39–43]. The interest in biochars as sorbents for the removal of a broad group of organic and inorganic pollutants is expanding. Thus, different biochars are extensively tested as “green” and sustainable sorbents. This is due mainly to their physicochemical properties, where biochars can be obtained within the pyrolysis of various biomass types or can be engineered through physical and chemical modifications [8,29]. Nanostructural biochar also reveals unique physicochemical properties over bulk biochar like high stability in various pH and temperature, high catalytic activity, and large specific surface area [44,45], while their properties are strictly dependent on the ageing method [46,47]. Biochars find a wide range of applications, especially in removing contaminants from aquatic systems [48]. The

literature reports a significant number of studies investigating the removal of antibiotics by plant-derived biochars [49–53]. There are also some studies on biochar derived from animal manure (e.g., bovine/cow manure, poultry manure) used to remove antibiotics and many other aquatic pollutants [40,54,55]. Although one can find many studies on the application of plant-derived biochars to remove various emerging contaminants from water or wastewater there is still insufficient data on biochars derived from animal manure, in particular from poultry manure, and their potential as sorbents for removing antibiotics and pigments from aquatic systems.

Thus, this research aims to address this gap in the current state of the art by investigating the potential of poultry manure-derived biochar for the removal of selected emerging contaminants, including antibiotics (such as tetracycline, TC) and pigments (such as rhodamine 6G, R6G). We analyzed the physical and chemical properties of poultry manure-derived biochar, including its carbon structure, and conducted adsorption studies to better understand the critical biochar properties and their effects on sorption efficiency. Based on the obtained results, the adsorption mechanism for TC and R6G on the investigated material is proposed.

2. Materials and methods

2.1. Chemicals

Rhodamine 6G (R6G) (95%) and tetracycline (TC) of the analytical grades were purchased from Sigma-Aldrich. NaOH, NaCl, and HCl were the analytical grades supplied from the POCHE Poland. Deionized water with a resistivity of 18.2 M Ω cm at 25°C was obtained using the Milli-Q ultra-pure water filtering system from Merck.

2.2. Production of biochar from poultry manure

Biochar was produced from poultry manure sampled from a local broiler house (Poland) with a cage rearing system. First, the sampled poultry manure was air-dried and crushed into smaller particles to get a homogeneous product. Then, it was transferred to a laboratory pyrolysis reactor (the PRW-S100 \times 780/11; manufactured by the Czylok company from Jastrzębie-Zdrój, Poland) and treated at the temperature of 725°C for 150 min under the nitrogen conditions with the rate of the gas flow of about 5 L min⁻¹. The pyrolysis temperature was selected based on the preliminary studies, prior the studies of biochars' sorption properties from poultry manure [47,48]. According to these preliminary studies biochar derived from poultry manure at the temperature of 725°C demonstrated required properties such as BET surface area, porosity and CEC that would assure higher sorption efficiency. Similar observations were reported in the most recent study on biochar [56]. The retention time was about 60 min. After the process of pyrolysis was completed, the obtained biochar was cooled down under the same conditions, and then placed onto the mesh with 500 μ m diameter porosity and washed with distilled water at the temperature of about 100°C for 30 min to remove potential crystals of salts that could form while

drying. Next, the biochar was washed with distilled water at room temperature. Finally, the biochar was placed in an oven and left for 24 h at 105°C.

2.3. Characterization of biochar

The morphology of the biochar sample was determined with the Scanning Electron Microscopy (SEM) — Merlin, ZEISS, Stuttgart, Germany. The BET surface area of poultry manure derived biochar was determined through nitrogen gas sorption by the ASAP 2020 Plus analyzer manufactured by Micromeritics (Atlanta, GA, USA) [48]. Biochar was analyzed for moisture content (by oven drying at 105°C) and ash following PN-EN ISO 18122:2016-01 [48]. The total carbon and total organic carbon content (TC and TOC) in the biochar were measured by multi N/C, Analytik Jena (high-temperature incineration with detection IR, Jena, Germany) according to the Polish standard PN-ISO 10694:2002 and Kjeldahl nitrogen content following the standard (PN-EN 16169:2012). The CHNS elemental analysis was performed with the Thermo Scientific™ FLASH 2000 (Waltham, MA, USA) method of dynamic incineration (3–4 independent incineration). The 5 g of the sample was placed into three individual beakers and then distilled water of about 50 mL was added to each of them to measure the pH of biochar. The samples were shaken for 10 min and then infiltrated. The pH was measured by a standard pH meter. The characterization of the carbon in the biochar was investigated by the Photoelectron spectroscopy (XPS) within the application of the GammaData Scienta from Uppsala, Sweden. The presence of organic compounds on the biochar surface was investigated by FT-IR spectroscopy with Nicolet 8700 Spectrometer (Thermo Scientific). The Raman spectroscopy was used complementary to the XPS to determine the graphitic character of the adsorbent. The spectra were collected using DXR Raman Microscopy (Thermo Scientific) with the 532 nm green laser line and 10 mm lenses. The exposure time was set to 30 s, and the signal was collected with 20 repetitions. The aperture was 50 μ m, the power of the laser beam was set at 5 mW. The UV-vis absorption spectra were recorded using a Perkin Elmer Lambda 35 ranging from 250 nm to 800 nm. The surface potential of the biochar was studied with Malvern Instruments Zetasizer Nano ZS, Malvern, UK.

2.4. Adsorption studies

The effectiveness of the tetracycline and rhodamine 6G removal from aqueous solutions was investigated using UV-vis spectrometry. The effect of pH was investigated by adjusting the pH of the respective solution of tetracycline (TC) and rhodamine 6G (R6G). Therefore, 7 mL of 70 mg L⁻¹ of the respective TC and R6G solutions were measured inside different beakers that contained 7 mg of the investigated biochar. Measurements were repeated three times. First, the pH of the mixture of each contaminant solutions and biochar inside beakers was adjusted to 2, 4, 6, 8 and 10 using dilute HCl and NaOH solutions and left for 19 h. Finally, the amount of TC and R6G left in the solution after 19 h was measured using a UV-vis spectrophotometer. The absorbance of TC and R6G was selected by UV-vis spectrometry technique considering the wavelength of

maximum absorbance which was 355 and 525 nm, respectively. Subsequently, the amount adsorbed onto biochar was calculated using equation 1.

$$A_a = \frac{(C_b - C_a)V}{m_a} \quad (1)$$

where A_a is amount of adsorbed compound (g), C_b and C_a in the equation stand for the concentration before and after adsorption (g L^{-1}), V is the volume of the solution (L), and m_a stands for the adsorbent mass. Apart from studying the pH on adsorption, we also analyzed the effect of contact time, ionic strength, adsorbate concentration, and the adsorbent dosage.

3. Results and discussion

3.1. Physical and chemical characterization of biochar

3.1.1. Morphology

The morphology of poultry manure derived biochar investigated with the scanning electron microscopy showed

a well-developed surface. The biochar occurs in irregular grains and flakes having different sizes and shapes. However, they have a rough surface for being coated with multiple tiny grain-like structures. These non-uniform nanostructures are visible in the sample, offering a large surface area. As shown in Fig. 1, the presented sample has an amorphous morphology where Fig. 1a shows the irregular shapes and sizes of the biochar, and Fig. 1b shows the nanostructures coating the biochars' structure. Fig. 1c shows the 3D image of biochar.

Moreover, the flake-like structures usually form graphitic carbon. Further analyses were performed to confirm the formation of a graphene-like structure. The morphology obtained for the biochar is similar to the morphology described in the literature for manure-based biochars [56].

3.1.2. BET isotherms

The specific surface area and micropore area of poultry manure derived biochar were investigated within the BET (i.e., Brunauer–Emmett–Teller) isotherms. The adsorption–desorption isotherms for the investigated biochar are presented in Fig. 2. The BET analysis shows that the active

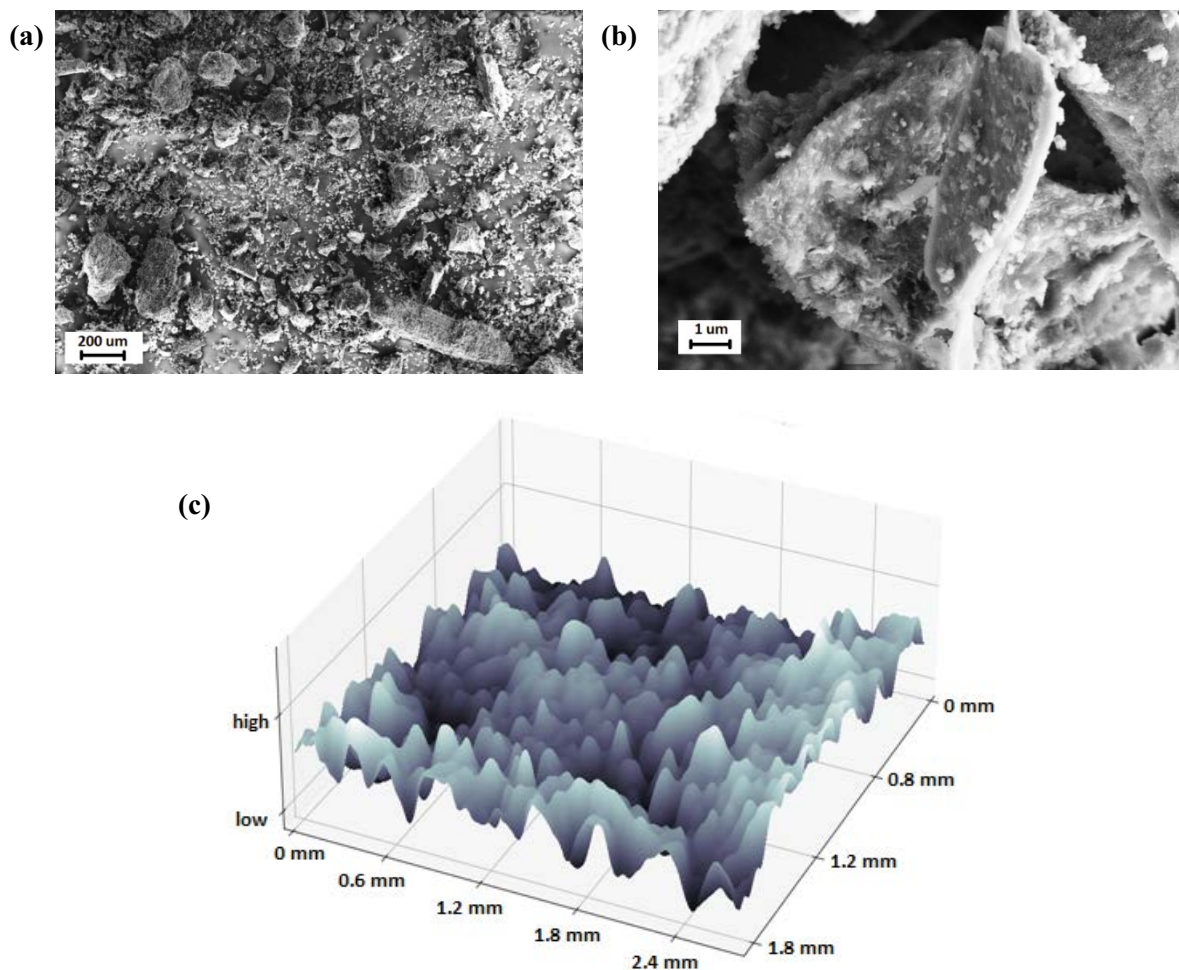


Fig. 1. SEM images of the biochar's morphology. Images (a,b) correspond to the same sample but at different scales and (c) 3D reconstruction of the biochar's surface.

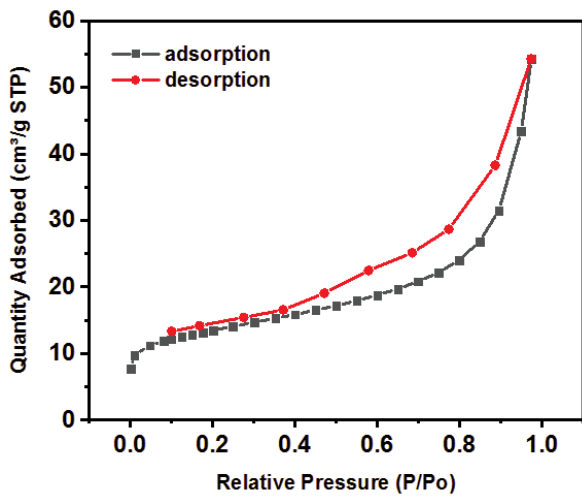


Fig. 2. The adsorption–desorption BET isotherm.

surface of the biochar was about $47.9136 \text{ m}^2 \text{ g}^{-1}$, the t-Plot Micropore Area was about $26.0085 \text{ m}^2 \text{ g}^{-1}$, and the t-Plot external surface area was about $27.3373 \text{ m}^2 \text{ g}^{-1}$. The single point adsorption for the total pore volume of pores was less than 74.8985 nm , and the width at $P/P_0 = 0.9742$ was about $0.08395 \text{ cm}^3 \text{ g}^{-1}$. The shape of the isotherm suggests the II type adsorbent where the tested biochar demonstrated macropores and a relatively flat surface and non-rigid plate aggregates classified by IUPAC (International Union of Pure and Applied Chemistry) as the H3 type sorbent. Such sorbents can be classified into type II which describes sorbents containing macropores or with a flat surface [42].

3.1.3. Characterization of the biochar – pH, moisture content, total organic carbon, and XPS analysis

Initially, the pH of the biochar was studied by soaking the material in distilled water and measurement with the use of pH-metric electrode. The obtained pH value of the biochar is alkaline with a pH of about 12.2, pointing out that the biochar has a significant potential for the sorption of positively charged compounds like antibiotics, dyes, and heavy metals. The moisture content of the dry mass was estimated experimentally at 0.45%, corresponding to the maximal water capacity in the pores of the particular biochar particles. In the total mass of the ash post pyrolysis, the entire carbon content was about 38.01%, while the total organic carbon was approximately 37.32%. The potassium content was about 3.42%, while the analysis also revealed the presence of some elements in the sample. Their content is as follows: Ca – 15.30%, P – 4.32%, K – 3.39%, Mg – 1.68%, 165 ppm of Cu, and 873 ppm of Zn. The pH and particular elements' content were measured within the procedure described in [48]. This complex composition will influence the final performance of the material.

Next, the biochar chemical composition was investigated with the X-ray photoelectron spectroscopy (XPS) where the deconvolution of high-resolution XPS spectra over the selected elements was conducted. Table 1 presents the atomic content in % for the investigated sample,

Table 1

The atomic content (%) for the investigated biochar

Name of element	Position (eV)	Atomic (%)
C 1s	284.57	56.05
O 1s	531.07	26.32
Ca 2s	438.52	4.71
N 1s	398.07	3.82
K 2p	292.51	2.15
P 2p	132.02	1.98
Mg 1s	1,303.07	1.64
Si 2p	102.06	1.14
S 2p	167.01	0.79
Cl 2p	197.53	0.78
Al 2p	75.01	0.35
Na 1s	1,071.52	0.26

indicating that carbon and oxygen are the main components of the biochar. Fig. 3 shows the high-resolution spectra for selected elements.

Fig. 3a presents the spectrum for the carbon, where the peak located at about 284.1 eV of C1s can be ascribed to the sp^2 and sp^3 [57]. The following peak at about 284.6 eV [58,59] is characteristic of C=C sp^2 being an aromatic form of carbon coming from the graphene-like structure. The C=C peak exhibits an asymmetric shape of the deconvoluted curve from the excitonic screening in sp^2 -conjugated in the graphene structure. Such domains can be observed in graphite and graphene in the highly reduced graphene oxide obtained at high temperatures [59]. Following peak at about 284.9 eV is characteristic of the C–H aliphatic carbon [58]. The peak centered at 285.5 eV can be related to the C–C sp^3 in the graphene. The recorded XPS spectrum also shows the appearance of the C–N peak centered at 285.9 eV. That peak overlaps with the following peak at about 286.4 eV which is characteristic of the C–OH in phenols [58,59]. The peak occurring at about 287.0 eV binding energy can be ascribed to the C–O–C [60] in the epoxy group that could form during pyrolysis in the sample. It can be also ascribed to the C–O–P for the carbon-oxygen-phosphorus chain. The presence of the carboxylic groups –COOH can be ascribed to the two following peaks located at about 288.0 eV and 288.8 eV where the first one corresponds to the C=O group and the second can be characteristic to the O=CO– group [59,61]. The XPS spectrum also reveals the presence of carbonates CO_3^{2-} at 289.6 eV and hydro-carbonates HCO_3^- where the peak is centered at 290.8 eV [61] quite often are present as residues in biochars [62].

The peak located at about 292.9 eV could be ascribed to the $\pi-\pi^*$ interactions in the carbon structure [61,63]. However, due to the presence of the following peak at about 295.5 eV it rather looks like the satellite peak and it can be ascribed to the presence of potassium in the sample. Both peaks can be ascribed to $\text{K}2\text{p}_{3/2}$ and $\text{K}2\text{p}_{1/2}$ respectively [64] that is a common element in biochars.

Next, Fig. 3b shows the spectrum recorded for oxygen where peaks characteristic of O 1s are seen. The high-resolution spectrum for that element is subdivided into four

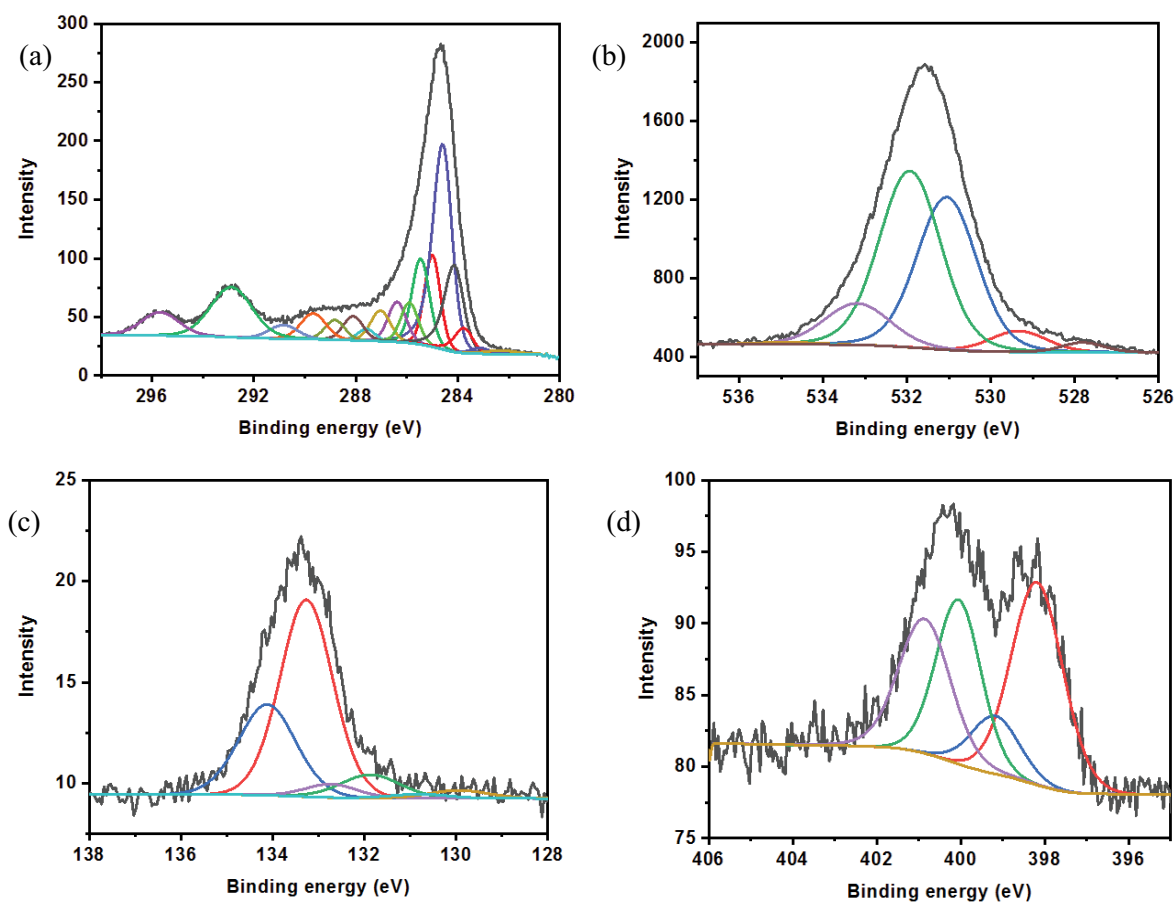


Fig. 3. The XPS spectra for (a) carbon, (b) oxygen, (c) phosphorus, and (d) nitrogen as obtained for biochar.

components where 529.3 eV can be attributed to the oxygen absorbed onto the surface of biochar or O^{2-} formation [65] or quinones $O=Ph=O$ [66]. The following peak at about 531.0 eV comes from the C–O bonding [60] where both the carboxyl $O=C-O$ [67] and carbonyl groups can ascribe [68]. It can also be attributed to the N–O [69] or deprotonated phosphates $P-O^-$ [70]. Next, the peak at 532.0 eV can be attributed to the C–O–H bonding, phosphorus-oxygen double bond $P=O$ [69], or carbonyl groups $C=O$ [69], while the peak at about 533.2 eV is characteristic carbonates or hydro-carbonates [65] being in the excellent agreement with the high-resolution spectrum for carbon.

Fig. 3c presents a high-resolution spectrum for phosphorus, clearly indicating particular peaks at about 131.9 eV from the P bonded to the aromatic ring $P-C_6H_5$ [71]. The following peaks at about 132.6 eV, 133.2 eV, and 134.1 eV can be ascribed to the phosphates like $Ca(H_2PO_4)_2$ or $Na_4P_2O_7$, respectively [71], wherein the region P 2p has several peaks.

The following spectrum presented in Fig. 3d is characteristic of nitrogen. The first peak at about 398.1 eV can be caused by the presence of the pyridinic-N like imine with sp^2 nitrogen in the biochar [72]. The peak at about 399.5 eV can be assigned to the $=N$ -bonds, while the following peaks at about 400.1 eV and 401.0 eV can be attributed to $-NH-$ and $-NH^+$, respectively [73,74].

As can be seen, carbon occurs in different forms. At the same time, the highest content is observed for aromatic carbon $C=C$ sp^2 , aliphatic carbon $C-H$ sp^3 , and $C-H$ sp^3 , suggesting that the biochar obtained within the pyrolysis at 725°C forms mainly the graphitic structure. The presence of oxygen can be ascribed primarily to the oxidized form of the carbon, while it is seen that biochar also contains traces of other elements like P, N, and Ca. Due to the presence of these elements, proposed biochar can also be used as a fertilizer, while P and N sites in the material can be proposed for the application of this material for catalytic studies in the environmental field.

3.1.4. Raman spectroscopy

Complementary to the XPS studies, the biochar was investigated and characterized by Raman spectroscopy [75] with consistent results from both methods. Based on that analysis, it was possible to confirm the carbon origin of the obtained sorbent and its structure [76]. The bands typical for the graphite and the amorphous carbon were present, in particular: ~ 482 cm^{-1} , $\sim 1,085$ cm^{-1} , $\sim 1,347$ cm^{-1} (D band), $\sim 1,576$ cm^{-1} (G band), $\sim 2,331$ cm^{-1} . The broadband $\sim 2,650$ – $29,00$ cm^{-1} includes the 2D band ($\sim 2,680$ cm^{-1}). One more peak, ~ 964 cm^{-1} , can probably be attributed to some traces

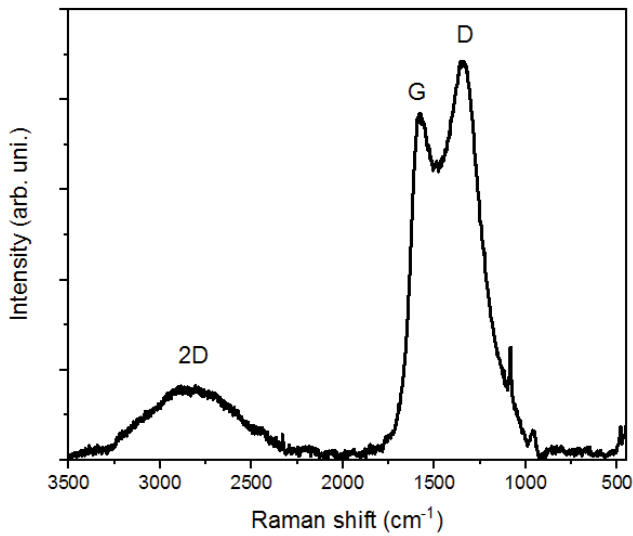


Fig. 4. The Raman spectrum confirms the presence of carbon in the biochar (532 nm).

of heteroatoms. One can observe in Fig. 4 that the 2D band is broad and weak. The residual compression stress can explain its shift towards higher frequencies.

Moreover, the intensity ratio $2D:G < 1$ indicates multilayered and not structuralized material. The G band is strongly shifted towards lower Raman shifts, and its half-width is $\sim 50 \text{ cm}^{-1}$ due to the low carrier concentration. The ratio $G:D \sim 0.25$ confirmed the high level of defects in the structure, which are crucial for the effective sorbent. The RBS parameter (Raman Band Separation) is relatively low and equal ~ 220 .

Based on the recorded spectrum it is seen that biochar has a non-uniform structure including defects. It can be an advantage of the material for the sorption of pollutants in the aquatic system.

3.2. Adsorption studies

3.2.1. Effect of the solution pH and biochar surface charge on the adsorption of tetracycline and rhodamine 6G

The amount of TC and R6G adsorbed at different pH values (2, 4, 6, 8, and 10) is shown in Fig. 5a and b, whereas

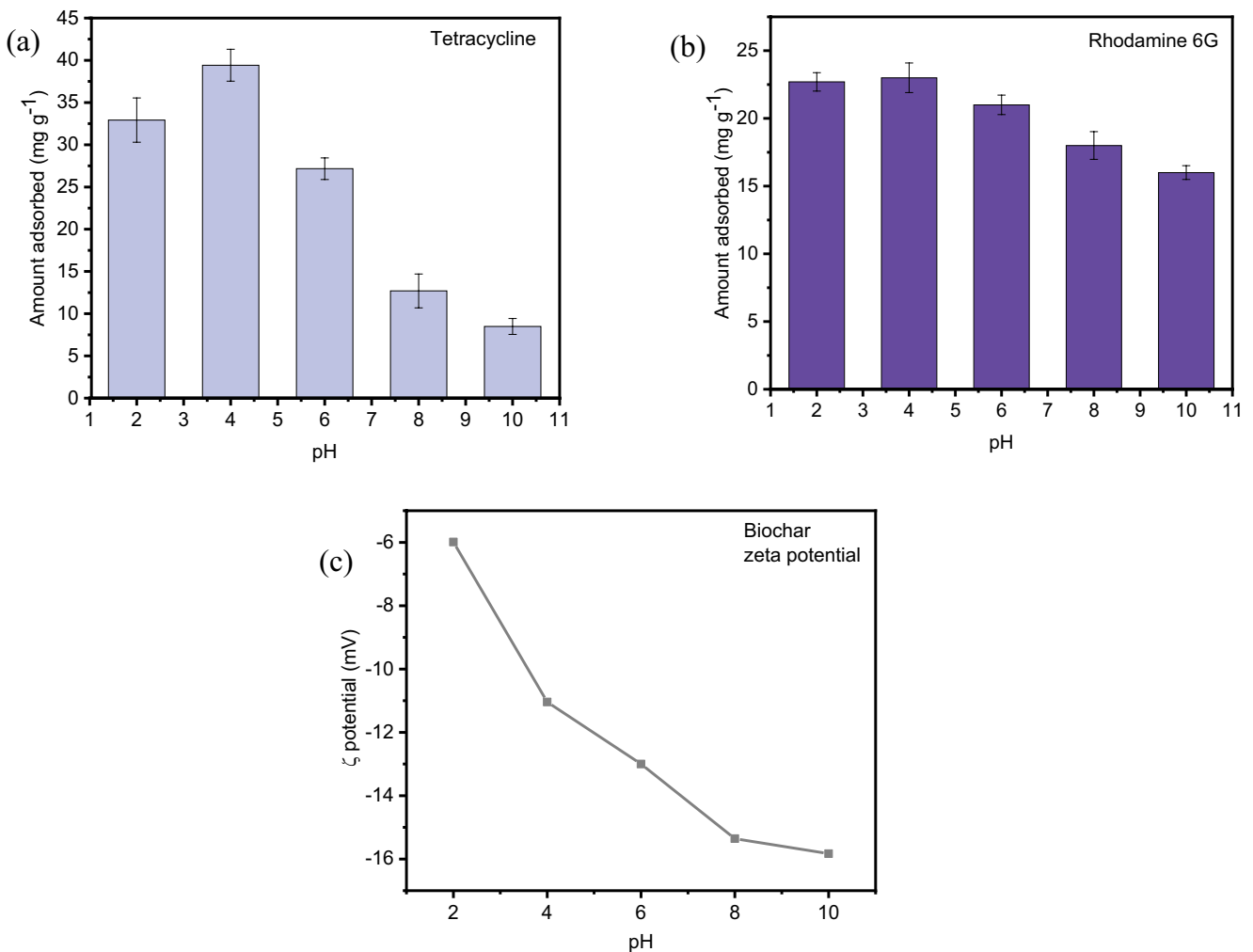


Fig. 5. The amount of absorbed tetracycline (a) and rhodamine 6G (b) in the pH range 2–10, and the zeta potential measurement of biochar (c).

Fig. 5c shows the surface charge of the biochar obtained by zeta potential measurement at the same pH values as during adsorption studies. The biochar has a negative surface charge which decreases with increasing pH from -6 mV to -16 mV. Thus, the hydrogen bonds have a negative effect on the zeta potential of the biochar. The presence of a negative surface charge is due to the deprotonation of the oxygen-containing functional group, such as $-\text{OH}$, $-\text{COOH}$, on the surface of the biochar, which increases in magnitude as the pH of the solution increases [77]. Moreover, the presence of alkaline substances (calcium carbonates, magnesium carbonates, etc.) which are left in biochar during production, and consequently contributed to a rise in pH when biochar was added to deionized water [78].

It is worth noting that TC consists of several pH-dependent structures that can be explained based on the acid-base equilibrium. The values of the acidity constants are $\text{p}K_1$ 3.3, $\text{p}K_2$ 7.7, and $\text{p}K_3$ 9.4. These values indicate that at acidic pH, TC is present in cationic species due to protonation of imine nitrogen, at pH between 3–7, it is present as zwitterionic species, in the range between 7–9 it is monoanionic, and finally, it is double anionic at $\text{pH} > 10$ [20,79]. In the case of Rhodamine 6G, it is a cationic dye [80]. The maximum amount of TC (39 mg g^{-1}) and R6G (23 mg g^{-1}) adsorbed is obtained at pH 4. In the case of TC, the amount adsorbed decreases at pH 6, 8 and 10 where the lowest amount adsorbed (8.5 mg g^{-1}) is obtained at pH 10. Similarly, the amount of R6G adsorbed decreased slightly in the same pH range (6, 8, 10). Since pH studies are important to present the largest sorption at certain conditions, from the practical point of view, the sorbent should be mainly applied in neutral or near-neutral media.

Therefore, relating the results obtained from the zeta potential of BC and the acid-base equilibrium of the tetracycline, one would expect electrostatic repulsion at pH 8 and 10. Instead, 12.7 and 8.5 mg g^{-1} were adsorbed at these pH values. These results suggest that the adsorption of TC on the biochar surface does not occur mainly through electrostatic interaction. However, its adsorption at acidic pH is due to the electrostatic attraction between cationic species (TC^+) and the negative surface of BC.

The rhodamine 6G is a cationic dye consisting of one carboxylic group and two amine groups. The results show adsorption of the dye at all pH values, reaching its maximum at pH 4, while at pH 6–10, the amount adsorbed slightly decreased. Since the biochar surface is negatively charged, the adsorption R6G is due to electrostatic interaction. Meanwhile, we expected that the adsorption of R6G would increase with rising pH. It is because of the negative values of the surface charge of BC with increasing pH. On the contrary, the amounts adsorbed at pH 6–10, were slightly lowered than at pH 2 and 4. The dissolution of mineral salts in the biochar resulted in the presence of Ca, Mg, Fe in the solution [78]. These cations could interfere with the adsorption of R6G, thereby leading to a slight reduction of the amount of R6G adsorbed at pH 6–10. More the deprotonation of the carboxylic group of R6G at alkaline pH resulting in the presence of COO^- , could as well lead to a slight decrease in the amount adsorbed.

3.2.2. Effect of contact time and adsorption kinetic

The results obtained from the effect of contact time on the adsorption of both TC and R6G are shown in Fig. 6a and b. The adsorption of the two contaminants at 5 min of contact time (based on the experimental data) was 21.7 and 18.4 mg g^{-1} for TC and R6G, respectively, and reached equilibrium at 240 min. The rapid adsorption process was due to the availability of the active sites at the early stage of the contact time. As the adsorption proceeded and more active sites were occupied by the adsorbed TC and R6G, the process slowed down until the equilibrium was attained. The data obtained were further treated by using nonlinear equations of the pseudo-first, pseudo-second and Elovich kinetic models. Since the value of R^2 has been used to determine the best model that is approximate to explain the reaction process. The R^2 obtained from pseudo-first, pseudo-second kinetic and Elovich models for the adsorption of TC, are 0.839, 0.908 and 0.981, respectively. In contrast, for the adsorption of R6G, they are 0.847, 0.932 and 0.981, respectively. This implies that it is more justified to relate the kinetic process with Elovich model. This model assumes

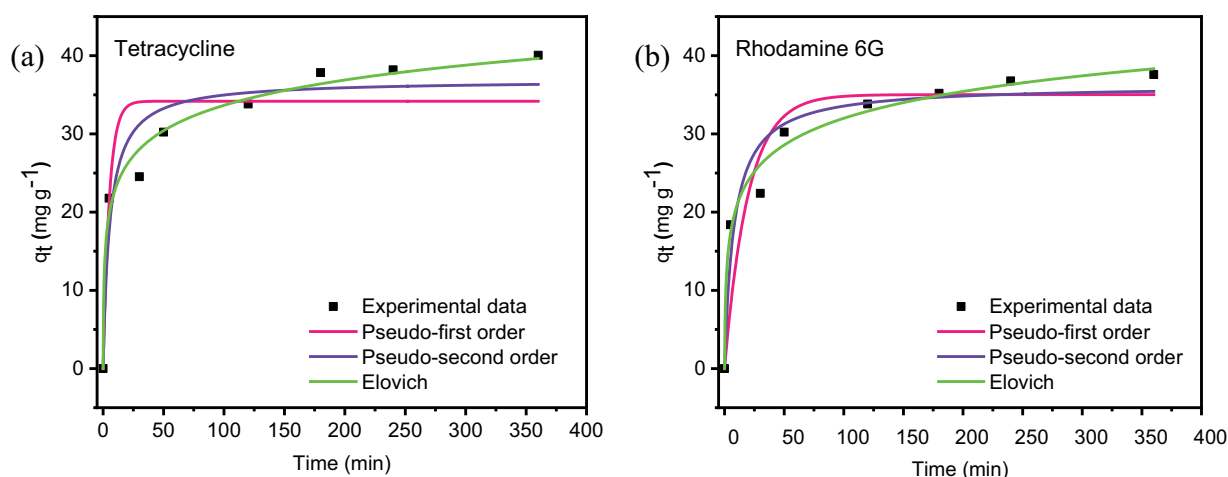


Fig. 6. Effect of contact time, kinetic plots of the adsorption of (a) TC and (b) R6G.

chemisorption and heterogeneous active sites, and that the rate of the amount adsorbed reduces as increases the surface of the adsorbent covered by the contaminants [81,82].

3.2.3. Effect of the initial concentration and adsorption isotherm

The initial concentration varied from 20 – 200 mg L⁻¹ for each investigated contaminant. The results are presented in Fig. 7a and b show that the adsorption increases with an increase in the initial concentration. It was observed that the increase in the initial concentration of the targeted contaminants contributes to the increase in the loading capacity of the adsorbent [83]. The data obtained were fitted into two commonly used isotherms that Langmuir and Freundlich proposed. The values of the correlation coefficient, R^2 obtained from Freundlich isotherm (0.985 for TC and 0.981 for R6G), are higher than Langmuir (0.978 for TC and 0.956 for R6G). Therefore, the adsorption of both TC and R6G are more consistent with Freundlich isotherm, which implies a heterogeneous adsorption process. Nevertheless, also an Elovich kinetics can be assigned. Since Langmuir isotherm gives the information on the maximum adsorption capacity of the adsorbent, the monolayer adsorption capacity of BC for the removal of TC and R6G are 65 and 63 mg g⁻¹, respectively. These values were compared with the results obtained for other adsorbents reported in the literature. As presented in Table 2, the investigated biochar demonstrated higher performance than some other adsorbents described in the literature.

3.2.4. Effect of the ionic strength

The effect of the ionic strength was studied at different concentrations of sodium chloride in the range of 0.025, 0.05, 0.075 and 0.1 M at pH 4 (at optimal pH for the adsorption of the two contaminants) and 100 mg L⁻¹ of TC and R6G. There is a slight increase in the amount of TC adsorbed when ionic strength increases (Fig. 8a). As discussed earlier, the electrostatic interaction plays a significant role in the adsorption of cationic species of TC on the surface of negatively

charged BC at pH 4. However, the presence of salt rather than inhibit the adsorption of TC, increases it slightly. The presence of salt in organic solution could increase the intermolecular, van der Waals' forces resulting in the aggregation of the organic molecules, thereby enhancing the adsorption process [84]. As shown in Fig. 8b, the addition of NaCl did not have any significant effect on the adsorption of R6G. This is because the presence of Na⁺ ions could neutralize the negative surface charge of the biochar, leading to electrostatic repulsion between biochar and R6G, meanwhile,

Table 2

Comparison of the maximum adsorption (q_{\max}) of different adsorbents for the removal of tetracycline and rhodamine 6G

Adsorbents	q_{\max} (mg g ⁻¹)	References
Tetracycline		
Fe ₃ O ₄ @C	14	[89]
Hydrous ferric oxide	41	[90]
R600	14	[91]
FeMn-BC	14.24	[92]
Cu-immobilized alginate	58	[93]
Magnetic porous carbon	25	[94]
Straw biochar	14.157	[95]
Bamboo charcoal	23.5	[96]
Bovine manure biochar	5.82	[40]
Poultry manure derived biochar	65	This study
Rhodamine 6G		
γ -Fe ₂ O ₃ /N-rGO	44	[97]
Graphene oxide	23.3	[98]
Activated carbon	44.7	[99]
Almond shell	32.6	[100]
Fe ₂ O ₃ /biochar	9.42	[101]
Date fibers	10.75	[102]
Graphene sand	55	[103]
Poultry manure derived biochar	63	This study

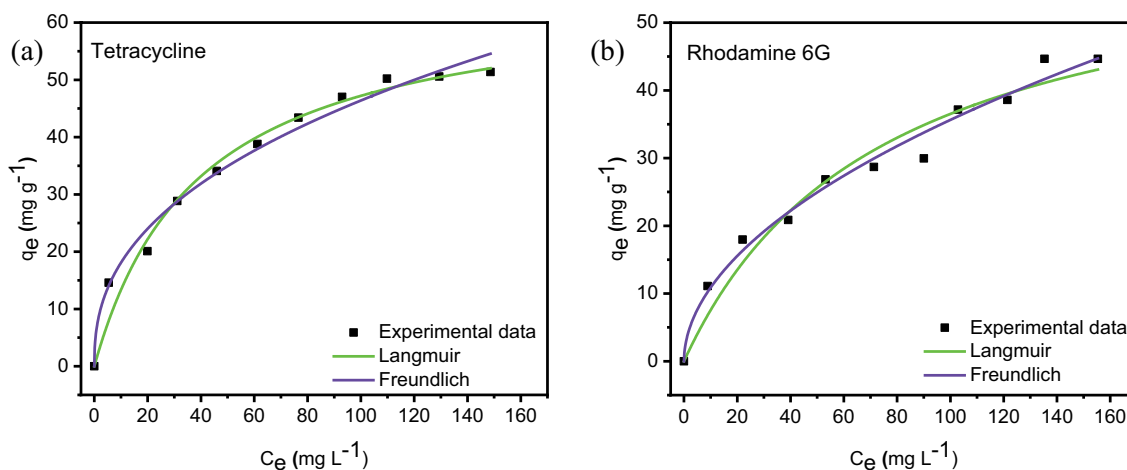


Fig. 7. Adsorption isotherms for removal of TC and R6G.

since electrostatic interaction was not the only mechanism through which BC adsorbed R6G, this led to the insignificant effect of sodium chloride on the adsorption process.

3.2.5. Effect of the adsorbent dosage

In this study, 100 mg L⁻¹ of each contaminant (TC and R6G) were prepared, out of which 7 mL was added to the separate beakers containing 3.5, 7, 10, 15 and 20 mg of the biochar to find the optimal dose of the TC and R6G treatment. The solutions in the respective beakers were adjusted to pH 4. The removal efficiency tends to increase as the number of adsorbent materials increases. In the case of both pollutants, there is an increasing sorption, starting from a minimum of 38% and 20% for TC and R6G, respectively, when 3.5 mg of the biochar was added (Fig. 9a and b). Then, reaching a maximum value of 62% and 60% for TC and R6G, respectively, when 20 mg of the biochar was added. These results can be explained as follows: as the biochar dosage increases, the surface-active sites of the adsorbent increase, leading to greater availability of active adsorbent sites to adsorb both tetracycline and rhodamine 6G from the aqueous solution.

3.2.6. Proposed mechanisms of adsorption

Based on the results obtained from the effect of pH, ionic strength and the information on the surface charge of BC, the mechanisms of adsorption of TC and R6G are due to the electrostatic attraction between the cation species of TC, cationic R6G and the negatively charged surface of BC. However, also other mechanisms are involved in the adsorption process. To ascertain this, the FTIR spectra of BC before and after adsorption of the two contaminants were measured and compared. These spectra are presented in Fig. 10a and b. In both cases, the spectrum of BC shows the presence of OH functional groups at 3,523 and 3,444 cm⁻¹. Especially, the peak at 3,444 cm⁻¹ is assigned to the OH stretching of hydrogen-bonded hydroxyl groups [85]. The peak at 1,462 cm⁻¹ is attributed to the presence of conjugated C=C of biochar aromatic rings [86,100]. The peak associated with C–O–C symmetric stretching in aliphatic groups is found at 1,040 cm⁻¹ [100]. The presence of carbonates or silicates is attributed to the appearance of peaks within 400–900 cm⁻¹ [87]. After the adsorption of TC and R6G the intensity of the peak at 1462 cm⁻¹ is reduced due to the interaction between the aromatic rings of BC and those of TC and R6G. According to

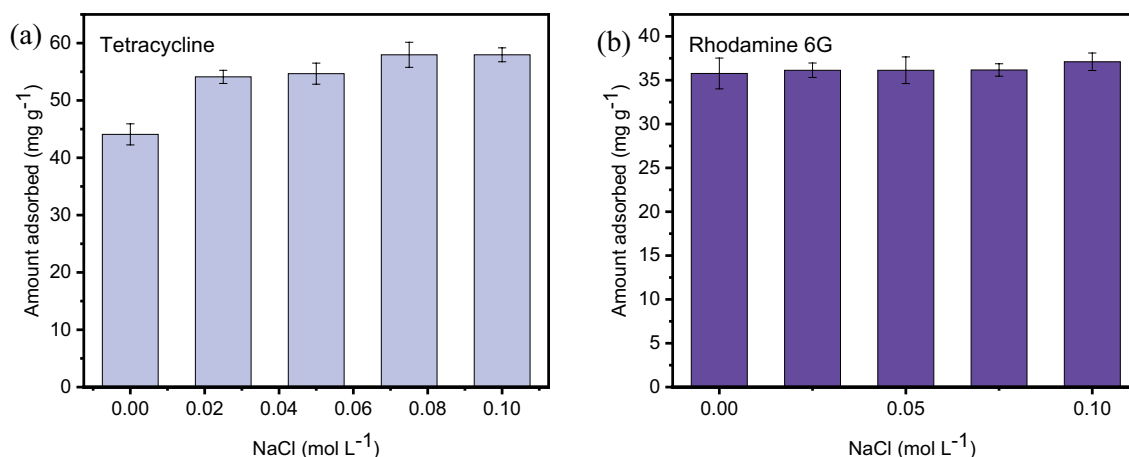


Fig. 8. Effect of the ionic strength on the adsorption of TC (a) and R6G (b) onto biochar.

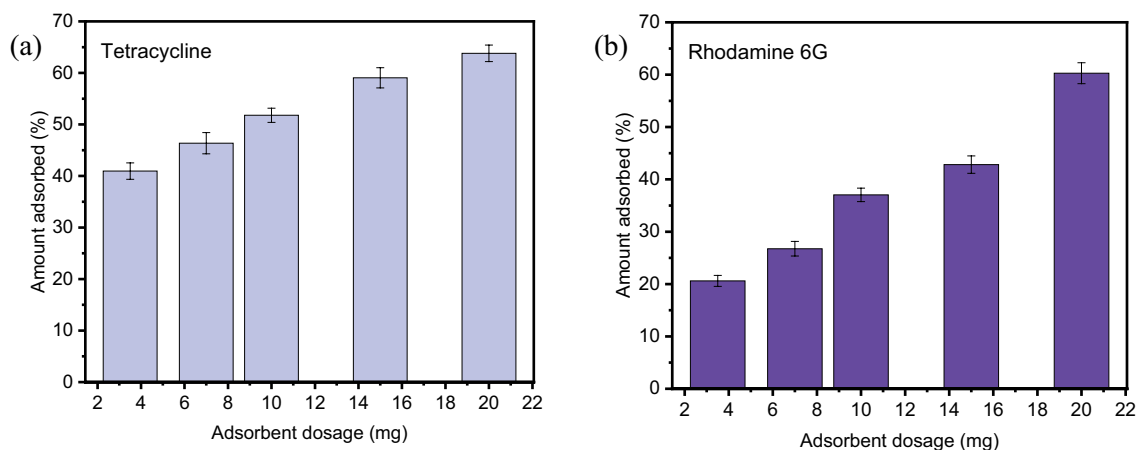


Fig. 9. Effect of adsorbent dosage on the adsorption of TC (a) and R6G (b) onto biochar.

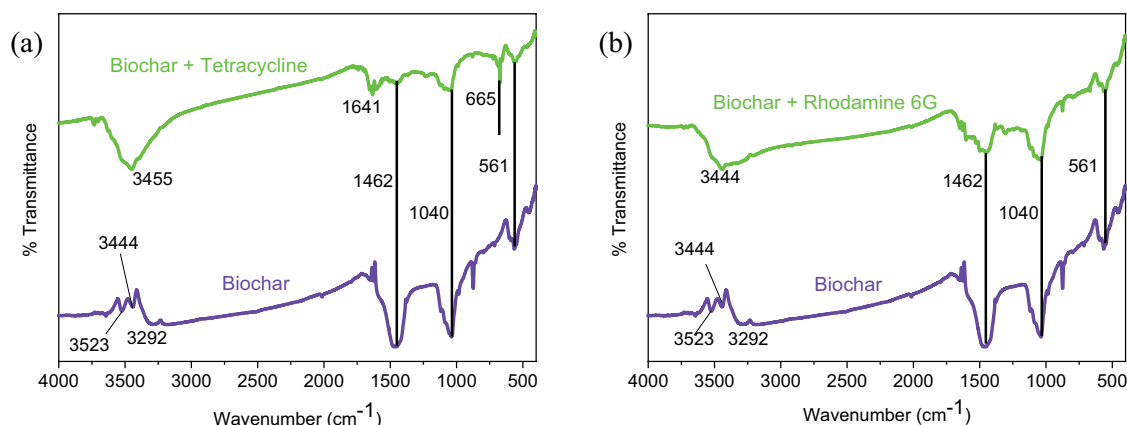


Fig. 10. The FTIR spectra of BC before and after adsorption of (a) TC and (b) R6G.

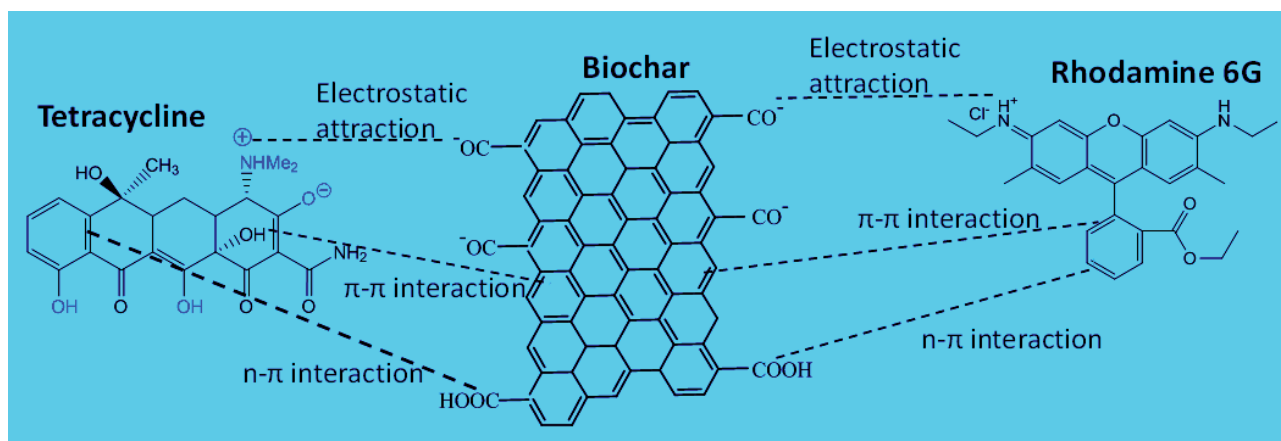


Fig. 11. Mechanisms of TC and R6G adsorption on biochar.

Tran et al. [82], this observation can be explained by the π - π interaction between the contaminants and BC. There is also a reduction in the intensity of the peak assigned to C-O-C after the adsorption of the two contaminants. This is due to n - π interaction between the oxygens (electron donors) in the carbonyl groups of BC and aromatic rings (electron acceptors) of TC and R6G [88]. The presence of peaks at 1,641 and 665 cm⁻¹ after the adsorption of TC indicates the presence of TC. The peaks at 3,523; 3,444 and 3,292 cm⁻¹ disappeared with the emergence of those at 3,455 and 3,444 cm⁻¹ after the adsorption of TC and R6G, respectively.

Given this, the mechanism of the adsorption of TC and R6G on the surface of BC is due to electrostatic attraction, π - π interaction and n - π interaction. The schematic mechanism is presented in Fig. 11.

4. Conclusions and future work

The investigated pristine biochar produced from poultry manure proved to be a promising adsorbent reaching over 60% efficiency for the removal of tetracycline and rhodamine 6G from an aqueous solution. One can point out that poultry manure derived biochar showed a pH of about 12.2, which proves that the biochar has a significant

potential for the sorption of positively charged compounds like medicines, pigments, and including heavy metal ions.

The adsorption efficiency depended on the initial concentration of TC and R6G, biochar dosage and pH. We observed that the adsorption capacity increased with the initial concentration of contaminants. The maximum amount of TC (39 mg g⁻¹) and R6G (23 mg g⁻¹) adsorbed is obtained at pH 4.

The obtained results suggest that the adsorption of TC on the biochar surface does not occur mainly through electrostatic interaction. However, its adsorption at acidic pH is due to the electrostatic attraction between cationic species (TC⁺) and the negative surface of BC. In view of this, the mechanism of TC and R6G adsorption on the surface of poultry manure derived biochar is mainly due to electrostatic attraction π - π interaction and n - π interaction.

Future work on poultry manure derived biochars should aim at: evaluating the effect of coexisting ions on the adsorption by biochar, analyzing the effect of physical and chemical modifications of biochar to increase the efficiency of the removal of selected contaminants both under laboratory conditions and real environments (e.g., wastewater treatment plants), and investigating the reusability of pristine and modified biochars obtained from pyrolysis of poultry manure.

Acknowledgements

M.M. would like to thank European Commission and Sapienza University in Rome for support within the Erasmus project. Furthermore, S.J.O. would like to thank the Polish National Agency for Academic Exchange (NAWA) for their support within the grant No PPN/U LM/2020/1/00051/DEC/01.M.O. and M.M. would like to thank prof. Michael Giersig from the Institute of Physical Chemistry for opening his laboratory to perform experiments. A.D. would like to thank prof. Barbara Pajys for the inspiring work atmosphere and affiliating with her research group and Piotr Machowski for his patience with my questions. This article was also a part of the Science Embassy project.

Funding

This work was performed within the Nutri2Cycle project, which has received funding from the European Union's Horizon 2020 research and innovation program under grant agreement No. 773682.

References

- [1] B. Senthil Rathi, P. Senthil Kumar, D.-V.N. Vo, Critical review on hazardous pollutants in water environment: occurrence, monitoring, fate, removal technologies and risk assessment, *Sci. Total Environ.*, 797 (2021) 149134, doi: 10.1016/j.scitotenv.2021.149134.
- [2] A. Inyinbor Adejumo, O. Adebisi Babatunde, P. Oluyori Abimbola, A. Adelani-Akande Tabitha, O. Dada Adewumi, A. Oreofe Toyin, Water Pollution: Effects, Prevention, and Climatic Impact, M. Glavan, Ed., *Water Challenges of an Urbanizing World*, InTechOpen, 2018, 72018, doi: 10.5772/intechopen.72018.
- [3] N. Ivanova, V. Gugleva, M. Dobрева, I. Pehlivanov, S. Stefanov, V. Andonova, Silver Nanoparticles as Multi-Functional Drug Delivery Systems, M.A. Farrukh, Ed., *Nanomedicines*, InTechOpen, 2016, doi: 10.5772/intechopen.80238.
- [4] S.Y. Wee, N.A.H. Ismail, D.E.M. Haron, F.M. Yusoff, S.M. Praveena, A.Z. Aris, Pharmaceuticals, hormones, plasticizers, and pesticides in drinking water, *J. Hazard. Mater.*, 424 (2022) 127327, doi: 10.1016/j.jhazmat.2021.127327.
- [5] A. Pereira, L. Silva, C. Laranjeiro, A. Pena, Assessment of human pharmaceuticals in drinking water catchments, tap and drinking fountain waters, *Appl. Sci.*, 11 (2021) 7062, doi: 10.3390/app11157062.
- [6] C. Liu, L. Tan, L. Zhang, W. Tian, L. Ma, A review of the distribution of antibiotics in water in different regions of China and current antibiotic degradation pathways, *Front. Environ. Sci.*, 9 (2021) 692298, doi: 10.3389/fenvs.2021.692298.
- [7] C. Manyi-Loh, S. Mamphweli, E. Meyer, A. Okoh, Antibiotic use in agriculture and its consequential resistance in environmental sources: potential public health implications, *Molecules*, 23 (2018) 795, doi: 10.3390/molecules23040795.
- [8] P. Krasucka, B. Pan, O. Yong Sik, D. Mohan, B. Sarkar, P. Oleszczuk, Engineered biochar – a sustainable solution for the removal of antibiotics from water, *Chem. Eng. J.*, 405 (2021) 126926, doi: 10.1016/j.cej.2020.126926.
- [9] B. Halling-Sørensen, G. Sengeløv, J. Tjørnelund, Toxicity of tetracyclines and tetracycline degradation products to environmentally relevant bacteria, including selected tetracycline-resistant bacteria, *Arch. Environ. Contam. Toxicol.*, 42 (2002) 263–271.
- [10] J. Jeong, W. Song, W.J. Cooper, J. Jung, J. Greaves, Degradation of tetracycline antibiotics: mechanisms and kinetic studies for advanced oxidation/reduction processes, *Chemosphere*, 78 (2010) 533–540.
- [11] H. Huang, J. Tang, K. Gao, R. He, H. Zhao, D. Werner, Characterization of KOH modified biochars from different pyrolysis temperatures and enhanced adsorption of antibiotics, *RSC Adv.*, 7 (2017) 14640–14648.
- [12] S.D. Richardson, C.S. Willson, K.A. Rusch, Use of Rhodamine water tracer in the marshland upwelling system, *Ground Water*, 42 (2004) 678–688.
- [13] Y. Huang, D. Wang, W. Liu, L. Zheng, Y. Wang, X. Liu, M. Fan, Z. Gong, Rapid screening of rhodamine B in food by hydrogel solid-phase extraction coupled with direct fluorescence detection, *Food Chem.*, 316 (2020) 126378, doi: 10.1016/j.foodchem.2020.126378.
- [14] L.F. Pinto, A.M. Montaña, C.P. González, G.C. Barón, Removal of rhodamine B in wastewater from the textile industry using geopolymeric material, *J. Phys.: Conf. Ser.*, 1386 (2019) 012040, doi: 10.1088/1742-6596/1386/1/012040.
- [15] M. Soylak, Y.E. Unsal, E. Yilmaz, M. Tuzen, Determination of rhodamine B in soft drink, waste water and lipstick samples after solid phase extraction, *Food Chem. Toxicol.*, 48 (2011) 1796–1799.
- [16] R. Jain, M. Mathur, S. Sikarwar, A. Mittal, Removal of the hazardous dye rhodamine B through photocatalytic and adsorption treatments, *J. Environ. Manage.*, 85 (2007) 956–964.
- [17] National Toxicology Program, NTP Toxicology and Carcinogenesis Studies of Rhodamine 6G (C.I. Basic Red 1) (CAS No. 989-38-8) in F344/N Rats and B6C3F1 Mice (Feed Studies), *Natl. Toxicol. Program Tech. Rep. Ser.*, 1989, pp. 1–192.
- [18] J. Hoslett, T.M. Massara, S. Malamis, D. Ahmad, I. van den Boogaert, E. Katsou, B. Ahmad, A. Ghazal, S. Simons, L. Wrobel, H. Jouhara, Surface water filtration using granular media and membranes: a review, *Sci. Total Environ.*, 639 (2018) 1268–1282.
- [19] V. Kumar, K.K. Jaiswal, M. Verma, M.S. Vlaskin, M. Nanda, P.K. Chauhan, A. Singh, H. Kim, Algae-based sustainable approach for simultaneous removal of micropollutants, and bacteria from urban wastewater and its real-time reuse for aquaculture, *Sci. Total Environ.*, 774 (2021) 145556, doi: 10.1016/j.scitotenv.2021.145556.
- [20] M. Nagamine, M. Osial, K. Jackowska, P. Kryszinski, J. Widera-Kalinowska, Tetracycline photocatalytic degradation under CdS treatment, *J. Mar. Sci. Eng.*, 8 (2020) 483, doi: 10.3390/jmse8070483.
- [21] A.K. Reddy, V.L. Reddy, E. Kwon, K.H. Kim, T. Akter, S. Kalagara, Recent advances in photocatalytic treatment of pollutants in aqueous media, *Environ. Int.*, 91 (2016) 94–103.
- [22] S.J. Olusegun, G. Larrea, M. Osial, K. Jackowska, P. Kryszinski, Photocatalytic degradation of antibiotics by superparamagnetic iron oxide nanoparticles. Tetracycline case, *Catalysts*, 11 (2021) 1243, doi: 10.3390/catal11101243.
- [23] V. Weber, I. Kamika, M.N.B. Momba, Comparing the effect of zinc oxide and titanium dioxide nanoparticles on the ability of moderately halophilic bacteria to treat wastewater, *Sci. Rep.*, 11 (2021) 16969, doi: 10.1038/s41598-021-96413-5.
- [24] P. Pietrzyk, N.T. Phuong, S.J. Olusegun, N. Hong Nam, D.T.M. Thanh, M. Giersig, P. Kryszinski, M. Osial, Titan yellow and Congo red removal with superparamagnetic iron-oxide-based nanoparticles doped with zinc, *Magnetochemistry*, 8 (2022) 91, doi: 10.3390/magnetochemistry8080091.
- [25] M. Abd Elkodous, G.S. El-Sayyad, S.M. Youssry, H.G. Nada, M. Gobara, M.A. Elsayed, A.M. El-Khawaga, G. Kawamura, W.K. Tan, A.I. El-Batal, A. Matsuda, Carbon-dot-loaded $\text{Co}_x\text{Ni}_{1-x}\text{Fe}_2\text{O}_4$; $x = 0.9/\text{SiO}_2/\text{TiO}_2$ nanocomposite with enhanced photocatalytic and antimicrobial potential: an engineered nanocomposite for wastewater treatment, *Sci. Rep.*, 10 (2020) 11534, doi: 10.1038/s41598-020-68173-1.
- [26] S.J. Olusegun, N.D.S. Mohalle, Comparative adsorption mechanism of doxycycline and Congo red using synthesized kaolinite supported CoFe_2O_4 nanoparticles, *Environ. Pollut.*, 260 (2020) 114019, doi: 10.1016/j.envpol.2020.114019.
- [27] D.L. Thi, T.P.T. Le, H.T. Do, H.T. Vo, N.T. Pham, T.T. Nguyen, H.T. Cao, P.T. Nguyen, T.M.T. Dinh, H.V. Le, D.L. Tran, Fabrication of porous hydroxyapatite granules as an effective adsorbent for the removal of aqueous Pb(II) ions, *J. Chem.*, 2019 (2019) 8620181, doi: 10.1155/2019/8620181.

- [28] L. Lu, J.S. Guest, C.A. Peters, X. Zhu, G.H. Rau, Z.J. Ren, Wastewater treatment for carbon capture and utilization, *Nat. Sustain.*, 1 (2018) 750–758.
- [29] N. Hossain, S. Nizamuddin, G. Griffin, P. Selvakannan, N.M. Mubarak, T.M.I. Mahlia, Synthesis and characterization of rice husk biochar via hydrothermal carbonization for wastewater treatment and biofuel production, *Sci. Rep.*, 10 (2020) 18851, doi: 10.1038/s41598-020-75936-3.
- [30] J. Sun, X. Liu, F. Zhang, J. Zhou, J. Wu, A. Alsaedi, H. Tasawar, J. Li, Insight into the mechanism of adsorption of phenol and resorcinol on activated carbons with different oxidation degrees, *Colloids Surf., A*, 563 (2019) 22–30.
- [31] W. Xiang, Y. Wan, X. Zhang, Z. Tan, T. Xia, Y. Zheng, B. Gao, Adsorption of tetracycline hydrochloride onto ball-milled biochar: governing factors and mechanisms, *Chemosphere*, 255 (2020) 127057, doi: 10.1016/j.chemosphere.2020.127057.
- [32] Y.X. Seow, Y.H. Tan, N.M. Mubarak, J. Kasedo, M. Khalid, M.L. Ibrahim, M. Ghasemi, A review on biochar production from different biomass wastes by recent carbonization technologies and its sustainable applications, *J. Environ. Chem. Eng.*, 10 (2022) 107017, doi: 10.1016/j.jece.2021.107017.
- [33] Y. Zhang, S. Fan, T. Liu, W. Fu, B. Li, A review of biochar prepared by microwave-assisted pyrolysis of organic wastes, *Sustainable Energy Technol. Assess.*, 50 (2022) 101873, doi: 10.1016/j.seta.2021.101873.
- [34] Q. Zhang, D. Zhang, W. Lu, M.U. Khan, H. Xu, W. Yi, H. Lei, E. Huo, M. Qian, Y. Zhao, R. Zou, Production of high-density polyethylene biocomposites from rice husk biochar: effects of varying pyrolysis temperature, *Sci. Total Environ.*, 738 (2020) 139910, doi: 10.1016/j.scitotenv.2020.139910.
- [35] Q. Shen, Z. Wang, Q. Yu, Y. Cheng, Z. Liu, T. Zhang, S. Zhou, Removal of tetracycline from an aqueous solution using manganese dioxide modified biochar derived from Chinese herbal medicine residues, *Environ. Res.*, 183 (2020) 109195, doi: 10.1016/j.envres.2020.109195.
- [36] F. Saremi, M.R. Miroliaei, M. Shahabi Nejad, H. Sheibani, Adsorption of tetracycline antibiotic from aqueous solutions onto vitamin B6-upgraded biochar derived from date palm leaves, *J. Mol. Liq.*, 318 (2020) 114126, doi: 10.1016/j.molliq.2020.114126.
- [37] H.M. Jang, S. Yoo, Y.K. Choi, S. Park, E. Kan, Adsorption isotherm, kinetic modeling and mechanism of tetracycline on *Pinus taeda* derived activated biochar, *Bioresour. Technol.*, 259 (2018) 24–31.
- [38] V.T. Nguyen, T.B. Nguyen, C.W. Chen, C.M. Hung, T.D.H. Vo, J.H.C. Chang, D. Dong, Influence of pyrolysis temperature on polycyclic aromatic hydrocarbons production and tetracycline adsorption behavior of biochar derived from spent coffee ground, *Bioresour. Technol.*, 284 (2019) 197–203.
- [39] P. Zhang, Y. Li, Y. Cao, L. Han, Characteristics of tetracycline adsorption by cow manure biochar prepared at different pyrolysis temperatures, *Bioresour. Technol.*, 285 (2019) 121348, doi: 10.1016/j.biortech.2019.121348.
- [40] J. Zhao, F. Gao, Y. Sun, W. Fang, X. Li, Y. Dai, New use for biochar derived from bovine manure for tetracycline removal, *J. Environ. Chem. Eng.*, 9 (2021) 105585, doi: 10.1016/j.jece.2021.105585.
- [41] D. Zhang, Q. He, X. Hu, K. Zhang, C. Chen, Y. Xue, Enhanced adsorption for the removal of tetracycline hydrochloride (TC) using ball-milled biochar derived from crayfish shell, *Colloids Surf., A*, 615 (2021) 126254, doi: 10.1016/j.colsurfa.2021.126254.
- [42] K. Wyslalska, K. Malińska, M. Barczak, Poultry manure derived biochars – the impact of pyrolysis temperature on selected properties and potentials for further modifications, *J. Sustain. Dev. Energy Water Environ. Syst.*, 9 (2021) 1080337.
- [43] J. Sobik-Szołtysek, K. Wyslalska, K. Malińska, E. Meers, Influence of pyrolysis temperature on the heavy metal sorption capacity of biochar from poultry manure, *Materials*, 14 (2021) 6566, doi: 10.3390/ma14216566.
- [44] B. Song, X. Cao, W. Gao, S. Aziz, S. Gao, C.H. Lam, R. Lin, Preparation of nano-biochar from conventional biorefineries for high-value applications, *Renewable Sustainable Energy Rev.*, 157 (2022) 112057, doi: 10.1016/j.rser.2021.112057.
- [45] K. Ghassemi-Golezani, S. Farhangi-Abriz, Improving plant available water holding capacity of soil by solid and chemically modified biochars, *Rhizosphere*, 21 (2021) 100469, doi: 10.1016/j.rhisph.2021.100469.
- [46] X. Yang, L. Wang, J. Guo, H. Wang, O. Mašek, H. Wang, N.S. Bolan, D.S. Alessi, D. Hou, Aging features of metal(loid)s in biochar-amended soil: effects of biochar type and aging method, *Sci. Total Environ.*, 815 (2022) 152922, doi: 10.1016/j.scitotenv.2022.152922.
- [47] Y. Liu, J. Chen, Effect of ageing on biochar properties and pollutant management, *Chemosphere*, 292 (2022) 133427, doi: 10.1016/j.chemosphere.2021.133427.
- [48] D.C.C. da S. Medeiros, C. Nzediegwu, C. Benally, S.A. Messele, J.H. Kwak, M.A. Naeth, Y.S. Ok, S.X. Chang, M. Gamal El-Din, Pristine and engineered biochar for the removal of contaminants co-existing in several types of industrial wastewaters: a critical review, *Sci. Total Environ.*, 809 (2021) 151120, doi: 10.1016/j.scitotenv.2021.151120.
- [49] A. Dutta, F. Defersha, Biochar, biomethane and biofertilizer from cord residue: a hybrid thermo-chemical and biochemical approach, *Energy*, 165 (2018) 370–384.
- [50] D. Cheng, H.H. Ngo, W. Guo, S.W. Chang, D.D. Nguyen, X. Zhang, S. Varjani, Y. Liu, Feasibility study on a new pomelo peel derived biochar for tetracycline antibiotics removal in swine wastewater, *Sci. Total Environ.*, 720 (2020) 137662, doi: 10.1016/j.scitotenv.2020.137662.
- [51] J. Dai, X. Meng, Y. Zhang, Y. Huang, Effects of modification and magnetization of rice straw derived biochar on adsorption of tetracycline from water, *Bioresour. Technol.*, 311 (2020) 123455, doi: 10.1016/j.biortech.2020.123455.
- [52] J. Eun Kim, S. Kant Bhatia, H. Jin Song, E. Yoo, H. Jin Jeon, J.Y. Yoon, Y. Yang, R. Gurav, Y.H. Yang, H.J. Kim, Y.K. Choi, Adsorptive removal of tetracycline from aqueous solution by maple leaf-derived biochar, *Bioresour. Technol.*, 306 (2020) 123092, doi: 10.1016/j.biortech.2020.123092.
- [53] Y. Zhou, X. Liu, Y. Xiang, P. Wang, J. Zhang, F. Zhang, J. Wei, L. Luo, M. Lei, L. Tang, Modification of biochar derived from sawdust and its application in removal of tetracycline and copper from aqueous solution: adsorption mechanism and modelling, *Bioresour. Technol.*, 245 (2017) 266–273.
- [54] B. Qiu, X. Tao, H. Wang, W. Li, X. Ding, H. Chu, Biochar as a low-cost adsorbent for aqueous heavy metal removal: a review, *J. Anal. Appl. Pyrolysis*, 155 (2021) 105081, doi: 10.1016/j.jaap.2021.105081.
- [55] H.Q. Li, J.T. Hu, Y. Meng, J.H. Su, X.J. Wang, An investigation into the rapid removal of tetracycline using multilayered graphene-phase biochar derived from waste chicken feather, *Sci. Total Environ.*, 603 (2017) 39–48.
- [56] C. Li, S. Xie, Y. Wang, R. Jiang, X. Wang, N. Lv, X. Pan, G. Cai, G. Yu, Y. Wang, Multi-functional biochar preparation and heavy metal immobilization by co-pyrolysis of livestock feces and biomass waste, *Waste Manage.*, 134 (2021) 241–250.
- [57] S. Osswald, G. Yushin, V. Mochalin, S.O. Kucheyev, Y. Gogotsi, Control of sp²/sp³ carbon ratio and surface chemistry of nanodiamond powders by selective oxidation in air, *J. Am. Chem. Soc.*, 128 (2006) 11635–11642.
- [58] M. Koinuma, H. Tateishi, K. Hatakeyama, S. Miyamoto, C. Ogata, A. Funatsu, T. Taniguchi, Y. Matsumoto, Analysis of reduced graphene oxides by X-ray photoelectron spectroscopy and electrochemical capacitance, *Chem. Lett.*, 42 (2013) 924–926.
- [59] M.K. Rabchinskii, S.A. Ryzhkov, D.A. Kirilenko, N.V. Ulin, M.V. Baidakova, V.V. Shnitov, S.I. Pavlov, R.G. Chumakov, D.Y. Stolyarova, B.N. Besedina, A.V. Shvidchenko, D.V. Potorochin, F. Roth, D.A. Smirnov, M.V. Gudkov, M. Brzhezinskaya, O.I. Lebedev, V.P. Melnikov, P.N. Brunkov, From graphene oxide towards aminated graphene: facile synthesis, its structure and electronic properties, *Sci. Rep.*, 10 (2020) 6902, doi: 10.1038/s41598-020-63935-3.
- [60] G. Ganguly, S. Sharma, P. Papakonstantinou, J. Hamilton, Probing the thermal deoxygenation of graphene oxide using high-resolution in situ X-ray-based spectroscopies, *J. Phys. Chem. C*, 115 (2011) 17009–17019.

- [61] J. Wei, G. Yuan, Y. Liu, D. Bi, L. Xiao, J. Lu, B.K.G. Theng, H. Wang, L. Zhang, X. Zhang, Assessing the effect of pyrolysis temperature on the molecular properties and copper sorption capacity of a halophyte biochar, *Environ. Pollut.*, 251 (2019) 56–65.
- [62] A. Tomczyk, Z. Sokołowska, P. Boguta, Biochar physicochemical properties: pyrolysis temperature and feedstock kind effects, *Rev. Environ. Sci. Biotechnol.*, 19 (2020) 191–215.
- [63] J. Heeg, U. Schubert, F. Küchenmeister, Surface chemistry of planarized silk-films studied by XPS, *Microchim. Acta*, 133 (2000) 113–117.
- [64] Z. Tan, L. Liu, H.Q. Zhang, Mechanistic study of the influence of pyrolysis conditions on potassium speciation in biochar “preparation-application” process, *Sci. Total Environ.*, 599–600 (2017) 207–216.
- [65] M. Gao, Y. Zhang, X. Gong, Z. Song, Z. Guo, Removal mechanism of di-n-butyl phthalate and oxytetracycline from aqueous solutions by nano-manganese dioxide modified biochar, *Environ. Sci. Pollut. Res.*, 25 (2018) 7796–7807.
- [66] Y.J. Oh, J.J. Yoo, Y.I. Kim, J.K. Yoon, H.N. Yoon, J.H. Kim, S.B. Park, Oxygen functional groups and electrochemical capacitive behavior of incompletely reduced graphene oxides as a thin-film electrode of supercapacitor, *Electrochim. Acta*, 116 (2014) 118–128.
- [67] L. Stobinski, B. Lesiak, A. Malolepszy, M. Mazurkiewicz, B. Mierzwa, J. Zemek, P. Jiricek, I. Bieloshapka, Graphene oxide and reduced graphene oxide studied by the XRD, TEM and electron spectroscopy methods, *J. Electron. Spectrosc. Relat. Phenom.*, 195 (2014) 145–154.
- [68] M.K. Rabchinskii, A.T. Dideikin, D.A. Kirilenko, M.V. Baidakova, V.V. Shnitov, F. Roth, S.V. Konyakhin, N.A. Besadina, S.I. Pavlov, R.A. Kuricyn, N.M. Lebedeva, P.N. Brunkov, A.Y. Vul, Facile reduction of graphene oxide suspensions and films using glass wafers, *Sci. Rep.*, 8 (2018) 14154, doi: 10.1038/s41598-018-32488-x.
- [69] C. Reshma, H. Harendrakrishnakumar, M. Raja, J.M. Gladis, A.M. Stephan, Sulfur-immobilized nitrogen and oxygen co-doped hierarchically porous biomass carbon for lithium-sulfur batteries: influence of sulfur content and distribution on its performance, *ChemistrySelect*, 2 (2017) 10484–10495.
- [70] M. Wagstaffe, A.G. Thomas, M.J. Jackman, M. Torres-Molina, K.L. Syres, K. Handrup, An experimental investigation of the adsorption of a phosphonic acid on the anatase TiO₂(101) surface, *J. Phys. Chem. C*, 120 (2016) 1693–1700.
- [71] <https://srdata.nist.gov/xps/>
- [72] K.N. Wood, S.T. Christensen, D. Nodlund, A.A. Dameron, C. Ngo, H. Dinh, T. Gennett, R. O’Hayre, S. Pelypenko, Spectroscopic investigation of nitrogen-functionalized carbon materials, *Surf. Interface Anal.*, 48 (2016) 283–292.
- [73] M. Raicopol, C. Andronescu, R. Atasei, A. Hanganu, L. Pilan, Post-polymerization electrochemical functionalization of a conducting polymer: diazonium salt electroreduction at polypyrrole electrodes, *J. Electrochem. Soc.*, 161 (2014) G103, doi: 10.1149/2.0871412jes.
- [74] C. Maddi, F. Bourquard, V. Barnier, J. Avila, M.-C. Asensio, T. Tite, C. Donnet, F. Garrelie, Nano-architecture of nitrogen-doped graphene films synthesized from a solid CN source, *Sci. Rep.*, 8 (2018) 3247, doi: 10.1038/s41598-018-21639-9.
- [75] K. Grodecki, Raman spectroscopy of graphene (Spektroskopia ramanowska grafenu), *Mater. Elektron.*, 41 (2013) 47–53 (in Polish).
- [76] L.M. Malard, M.A. Pimenta, G. Dresselhaus, M.S. Dresselhaus, Raman spectroscopy in graphene, *Phys. Rep.*, 473 (2009) 51–87.
- [77] Z. Tan, S. Yuan, M. Hong, L. Zhang, Q. Huang, Mechanism of negative surface charge formation on biochar and its effect on the fixation of soil Cd, *J. Hazard. Mater.*, 384 (2020) 121370, doi: 10.1016/j.jhazmat.2019.121370.
- [78] J.H. Yuan, R.K. Xu, H. Zhang, The forms of alkalis in the biochar produced from crop residues at different temperatures, *Bioresour. Technol.*, 102 (2011) 3488–3497.
- [79] W. Zuo, N. Li, B. Chen, C. Zhang, Q. Li, M. Yan, Investigation of the deprotonation of tetracycline using differential absorbance spectra: a comparative experimental and DFT/TD-DFT study, *Sci. Total Environ.*, 726 (2020) 138432, doi: 10.1016/j.scitotenv.2020.138432.
- [80] S. Rajoriya, S. Bargole, V.K. Saharan, Degradation of a cationic dye (Rhodamine 6G) using hydrodynamic cavitation coupled with other oxidative agents: Reaction mechanism and pathway, *Ultrason. Sonochem.*, 34 (2017) 183–194.
- [81] S.J. Olusegun, E.T.F. Freitas, L.R.S. Lara, H.O. Stumpf, N.D.S. Mohallem, Effect of drying process and calcination on the structural and magnetic properties of cobalt ferrite, *Ceram. Int.*, 45 (2019) 8734–8743.
- [82] H.N. Tran, S.-J. You, A. Hosseini-Bandegharai, H.P. Chao, Mistakes and inconsistencies regarding adsorption of contaminants from aqueous solutions: a critical review, *Water Res.*, 120 (2017) 88–116.
- [83] M.A. Al-Ghouti, R.S. Al-Absi, Mechanistic understanding of the adsorption and thermodynamic aspects of cationic methylene blue dye onto cellulosic olive stones biomass from wastewater, *Sci. Rep.*, 10 (2020) 15928, doi: 10.1038/s41598-020-72996-3.
- [84] M.K. Gofar, K. Moradi, N.M. Kor, N. Moradi, Spectroscopic studies on aggregation phenomena of dyes, *Eur. J. Exp. Biol.*, 4 (2014) 72–81.
- [85] J. Rainer, V. Mrlik, R. Doris, H. Jakub, P. Sedlacek, B. Lucie, G. Soja, Biochar surface functional groups as affected by biomass feedstock, biochar composition and pyrolysis temperature, *Carbon Resour. Convers.*, 4 (2021) 36–46.
- [86] Y. Cuixia, X. Yingming, W. Lin, L. Xuefeng, S. Yuebing, Effect of different pyrolysis temperatures on physico-chemical characteristics and lead(II) removal of biochar derived from chicken manure, *RSC Adv.*, 10 (2020) 3667–3674.
- [87] L. Liu, G. Liu, J. Zhou, J. Wang, A. Wang, Improved bioreduction of nitrobenzene by black carbon/biochar derived from crop residues, *RSC Adv.*, 6 (2016) 84388–84396.
- [88] H.N. Tran, S.J. You, T.V. Nguyen, H.P. Chao, Insight into the adsorption mechanism of cationic dye onto biosorbents derived from agricultural wastes, *Chem. Eng. Commun.*, 204 (2017) 1020–1036.
- [89] V. Soares, M.C. Grando, G.L. Colpani, L.L. Silva, J. Maria, M.D.M. Mello, Obtaining of Fe₃O₄@C core-shell nanoparticles as an adsorbent of tetracycline in aqueous solutions, *Mater. Res.*, 22 (2019) 1–11.
- [90] J. Zang, T. Wu, H. Song, N. Zhou, S. Fan, Z. Xie, J. Tang, Removal of tetracycline by hydrous ferric oxide: adsorption kinetics, isotherms, and mechanism, *Int. J. Environ. Res. Public Health*, 16 (2019) 4580, doi: 10.3390/ijerph16224580.
- [91] H. Wang, C. Fang, Q. Wang, Y. Chu, Y. Song, Y. Chen, X. Xue, Sorption of tetracycline on biochar derived from rice straw and swine manure, *RSC Adv.*, 8 (2018) 16260–16268.
- [92] X. Zhang, Y. Li, M. Wu, Y. Pang, Z. Hao, M. Hu, R. Qiu, Enhanced adsorption of tetracycline by an iron and manganese oxides loaded biochar: kinetics, mechanism and column adsorption, *Bioresour. Technol.*, 320 (2021) 124264, doi: 10.1016/j.biortech.2020.124264.
- [93] X. Zhang, X. Lin, Y. He, Y. Chen, X. Luo, R. Shang, Study on adsorption of tetracycline by Cu-immobilized alginate adsorbent from water environment, *Int. J. Biol. Macromol.*, 124 (2019) 418–428.
- [94] X. Zhu, Y. Liu, F. Qian, C. Zhou, S. Zhang, J. Chen, Bioresource technology preparation of magnetic porous carbon from waste hydrochar by simultaneous activation and magnetization for tetracycline removal, *Bioresour. Technol.*, 154 (2014) 209–214.
- [95] H. Wang, Y. Chu, C. Fang, F. Huang, Y. Song, X. Xue, Sorption of tetracycline on biochar derived from rice straw under different temperatures, *PLoS One*, 12 (2017) e0182776, doi: 10.1371/journal.pone.0182776.
- [96] P. Liao, Z. Zhan, J. Dai, X. Wu, W. Zhang, K. Wang, S. Yuan, Adsorption of tetracycline and chloramphenicol in aqueous solutions by bamboo charcoal: a batch and fixed-bed column study, *Chem. Eng. J.*, 228 (2013) 496–505.
- [97] L. Yang, J. Hu, L. He, J. Tang, Y. Zhou, J. Li, K. Ding, One-pot synthesis of multifunctional magnetic N-doped graphene composite for SERS detection, adsorption separation and photocatalytic degradation of Rhodamine 6G, *Chem. Eng. J.*, 327 (2017) 694–704.

- [98] H. Ren, D.D. Kulkarni, K. Rajesh, W. Xu, I. Choi, Competitive adsorption of dopamine and Rhodamine 6G on the surface of graphene oxide, *ACS Appl. Mater. Interfaces*, 6 (2014) 2459–2470.
- [99] G. Annadurai, R. Juang, D. Lee, Adsorption of rhodamine 6G from aqueous solutions on activated carbon, *J. Environ. Sci. Health., Part A*, 4529 (2007) 715–725.
- [100] H.B. Senturk, D. Ozdes, C. Duran, Biosorption of Rhodamine 6G from aqueous solutions onto almond shell (*Prunus dulcis*) as a low cost biosorbent, *Desalination*, 252 (2010) 81–87.
- [101] E.P. Santos, R.F. Silva, J.F. Silva, T. Suwunwong, P. Patho, P. Choto, K. Phoungthong, Enhancement the rhodamine 6G adsorption property on Fe₃O₄-composited biochar derived from rice husk, *Mater. Res. Express*, 7 (2020) 025511, doi: 10.1088/2053-1591/ab6b58.
- [102] A. Alizadeh, A. Parizanganeh, A. Zamani, Application of cellulosic biomass for removal of cationic dye Rhodamine 6G from aqueous solutions, *Int. J. Waste Resour.*, 6 (2016) 100256, doi: 10.4172/2252-5211.1000256.
- [103] S.S. Gupta, T.S. Sreepasad, S.M. Maliyekkal, S.K. Das, T. Pradeep, Graphene from sugar and its application in water purification, *ACS Appl. Mater. Interfaces*, 4 (2012) 4156–4163.